Soft Matter

PAPER

Cite this: *Soft Matter*, 2022, **18**, 446

Stress relaxation in network materials: the contribution of the network

S. N. Amjad and R. C. Picu *

Stress relaxation in network materials with permanent crosslinks is due to the transport of fluid within the network (poroelasticity), the viscoelasticity of the matrix and the viscoelasticity of the network. While relaxation associated with the matrix was studied extensively, the contribution of the network remains unexplored. In this work we consider two and three-dimensional stochastic fiber networks with viscoelastic fibers and explore the dependence of stress relaxation on network structure. We observe that relaxation has two regimes – an initial exponential regime, followed by a stretched exponential regime – similar to the situation in other disordered materials. The stretch exponent is a function of density, fiber diameter and the network structure, and has a minimum at the transition between the affine and non-affine regimes of network behavior. The relaxation time constant of the first, exponential regime is similar to the relaxation time constant of individual fibers and is independent of network density and fiber diameter. The relaxation time constant of the second, stretched exponential regime is a weak function of network parameters. The stretched exponential emerges from the heterogeneity of relaxation dynamics on scales comparable with the mesh size, with higher heterogeneity leading to smaller stretch exponents. In composite networks of fibers whose relaxation time constant is selected from a distribution with set mean, the stretch exponent decreases with increasing the coefficient of variation of the fiber time constant distribution. As opposed to thermal glass formers and colloids, in these athermal systems the dynamic heterogeneity is introduced by the network structure and does not evolve during relaxation. While in thermal systems the control parameter is the temperature, in this athermal case the control parameter is a non-dimensional structural parameter which describes the degree of non-affinity of the network.

Received 29th October 2021,
Accepted 10th December 2021

DOI: 10.1039/d1sm01546j

rsc.li/soft-matter-journal

1. Introduction

Many biological and soft man-made materials can be classified as network materials. This class includes materials in which a network of filaments provides structural integrity and controls the mechanical behavior, such as in cartilage, tendons, various membranes within the human body, gels, molecular networks such as elastomers, paper and nonwovens. Most of these materials exhibit time-dependent behavior. They may creep under constant load, relax after an imposed deformation when held at constant strain or, in general, exhibit strain rate-dependent stress in a generic mechanical test.

Multiple mechanisms lead to time dependence of the mechanical behavior of network materials, including: the time dependence of the matrix (if the network is embedded in a viscoelastic material), *e.g.*,[1] the transport of solvent across, and in and out of the network,[2,3] viscous interactions between filaments in contact,[4] the time dependence of the fiber material behavior, and the process of crosslink rupture or dissociation.[5,6] The last mechanism is inactive in permanently crosslinked networks. Viscous friction between filaments is essential in molecular networks with small free volume (*i.e.* when filaments are densely packed) such as in elastomers.[4,7] If the network is embedded in a viscoelastic matrix, the matrix contributes to the time dependence of the material behavior, an example being connective tissue which has polar and hydrophilic glycosaminoglycan molecules (GAG) embedded in the collagen network.[8] The transport of viscous fluid across the network introduces strain rate dependence, which is quantified by poroelastic models.[9,10] The characteristic time constant of relaxation within poroelasticity is proportional to the viscosity of the embedding fluid, η, and to the square of the sample size, and inversely proportional to the network stiffness, E_0. Finally, the time dependent behavior of individual filaments is also expected to contribute to the time dependence of the network response, but this aspect was not studied extensively to date.[11,12]

Collagen-based biological tissue is an intensely studied system in which multiple mechanisms operate. Stress

Department of Mechanical, Aerospace and Nuclear Engineering, Rensselaer Polytechnic Institute, Troy, NY 12180, USA. E-mail: picuc@rpi.edu; Tel: +1 518 276-2195

relaxation in reconstituted collagen was described with a Prony series with three time constants.[13–15] The values of these constants vary from report to report, but fall in the range 0.6–8 s, 13–40 s and 800–1300 s, respectively. Stress relaxation of collagenous tissue may be also described using a Prony series with three terms. In[16] the time constants reported for the rabbit periodontal ligament are 0.4 s, 4 s and 400 s, while in[17] the time constants for fibroblast-seeded collagen are approximately 10 s, 100 s and 2000 s. These works do not associate the relaxation modes with specific mechanisms. However, it is acknowledged that poroelasticity operates in all cases and is responsible for at least one of the relaxation modes.

An example in which one mechanism is clearly dominant is provided by chemical gels, such as acrylamide. The large free volume of chemical gels limits the direct interaction of filaments which implies that poroelasticity is more important than internal friction. A large number of publications present data for various gels, *e.g.*[18–21]

The mechanisms associated with solvent transport and the viscoelasticity of the embedding matrix do not operate in nonwovens and hence such materials may provide a testbed for the effectiveness of the other mechanisms causing time-dependent behavior listed above. Unfortunately, the literature on nonwovens does not support a unique conclusion in this sense, as some reports indicate that the network exhibits little or no time-dependent behavior despite the fact that individual fibers have time-dependent response,[22] while some other reports indicate the opposite. For example, ref. 23 reports logarithmic relaxation for a network of polycaprolactone fibers.

It becomes apparent that the broad range of behaviors reported in the literature on various network materials is due to the concomitant operation of multiple mechanisms. This makes difficult the evaluation of the contribution of individual mechanisms to global relaxation exclusively based on experimental data. As indicated above, of the various mechanisms, the effect of the time-dependent fiber behavior is the least studied and, in fact, rarely mentioned in discussions of the viscoelasticity of network materials. In order to isolate the contribution of the network to global relaxation, we construct in this work models in which all other relaxation mechanisms are absent. In these models fibers are viscoelastic and are characterized by a single relaxation time. Fiber interaction at sites which are not crosslinks is neglected. The crosslinks are permanent. We observe that the stochastic structure of the network introduces a slow relaxation regime of Kohlrausch type and study the dependence of the slowdown on the structural parameters of the network. It results that networks in the transition regime between affine and non-affine exhibit the most heterogeneous dynamics, which leads to maximum slowdown. This behavior, which is broadly encountered in thermal systems such as monatomic and polymeric glasses close to the glass transition temperature (T_g), is encountered here in a purely athermal system and is due to the frozen structural heterogeneity of the network.

2. Models and network structural parameters

Two (2D) and three-dimensional (3D) networks of Mikado and Voronoi type, respectively, are considered in this work. Such networks are widely used in the literature as proxies for network materials of 3D[24–26] and quasi-2D[27–29] types.

Mikado networks, Fig. 1a, are constructed by depositing fibers of length L_0 in a square problem domain of dimensions L. The fiber center of mass and their orientation are defined by random variables uniformly distributed over the problem domain and over the angular range $[0, \pi]$, respectively. Fibers are crosslinked at all points where they cross and the crosslinks are assumed to transmit both forces and moments (weld type) both along given fiber and from fiber to fiber. The connectivity number, *i.e.* the number of fiber segments emerging from each crosslink is $z = 4$. Dangling ends are eliminated since, as long as inter-fiber contacts are neglected, they do not contribute to the mechanics of the network. Since the crosslinks located at the fiber ends have $z = 3$, the overall connectivity index of the network is somewhat smaller than 4.

Voronoi networks, Fig. 1b, are constructed in cubic domains of edge length L by starting with randomly distributed seed points, which are used to tessellate the space using the Voronoi procedure. The edges of the polyhedral domains of the tesselation are retained as fibers. The fiber length is controlled by adjusting the number density of seed points. Each fiber has 2 crosslinks, one at each end. As in the Mikado network case, the crosslinks are of welded type and transmit both forces and moments. The connectivity of this network is $z = 4$.

In both Mikado and Voronoi networks, fibers have diameter, d, and viscoelastic behavior described by a Maxwell model of stiffness E_f and relaxation time constant τ_f. With the exception of the systems discussed in Section 3.4, all fibers in given model have same E_f and τ_f. In these cases, τ_f is considered the unit of time of the relaxation problem (*i.e.* it is used to normalize all relevant times). The unit of stress is E_f.

In order to study their relaxation, networks are loaded in uniaxial tension up to strain ε_0, after which the global strain is kept constant and the stress in the loading direction is monitored, $\sigma(t)$. Tractions in directions perpendicular to the loading direction are kept zero. The network is forced to deform in a linear elastic (although not necessarily affine) way up to ε_0, such

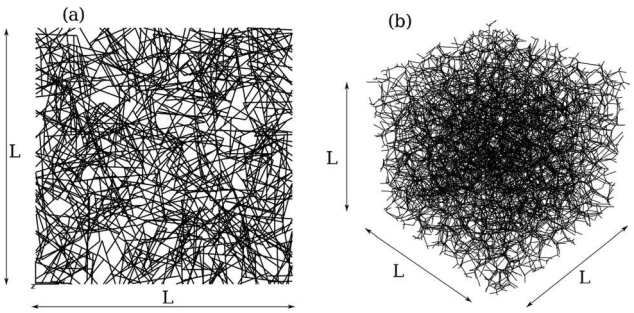

Fig. 1 (a) Mikado and (b) Voronoi networks used in this study.

to prevent relaxation during loading. To this end, the constitutive behavior of fibers is taken linear elastic up to the end of the loading period. The constitutive description is then switched to viscoelastic to trace the subsequent relaxation. The stress at the end of the loading period is denoted by σ_0. In most simulations reported here, ε_0 = 3%. Larger ε_0, up to 30%, are considered in order to determine to what extent structural changes introduced by the large imposed strains modify the relaxation behavior, and the results are reported in Section 3.3.

Fibers are modeled using Timoshenko beam elements (B22 in 2D and B32 in 3D) and the solution is obtained with the commercial finite element software Abaqus/Standard (version 62.3). In average 5 elements are used per fiber, discretization which led in previous studies to adequate convergence of the energy, and hence provides the best compromise between accuracy and computational cost.

One of the main goals of the present work is to establish the relation between network structural parameters and the relaxation behavior. Therefore, it is necessary to review the parameters used to describe the structure. The network density, ρ, is defined as the total length of fiber per unit area (in 2D) or volume (in 3D). In both Mikado and Voronoi networks, the segment lengths are Poisson distributed; the mean value, l_c, is the only parameter of this distribution. l_c is related to ρ as $\rho l_c = \pi/2$ in the Mikado case,[30] and as $\rho l_c^2 = c$ in the Voronoi case, where c = 0.95 for the unperturbed Voronoi network of straight fibers.[31] If fibers are not straight, c depends on fiber crimp,[32] as well as on any geometric perturbation applied to the basic Voronoi structure.[31]

At constant l_c, increasing the fiber diameter, d, increases the bending rigidity faster than the axial rigidity, which makes the axial mode gradually energetically less expensive than the bending mode. It is broadly reported in the literature on network mechanics[27,33,34] that dense networks of fibers with large d store most of the strain energy in the axial deformation mode of fibers. Consequently, such structures deform approximately affinely. Decreasing ρ and/or d leads to networks whose deformation is controlled by the bending mode of fibers and which exhibit non-affine deformation patterns. Network stiffness scales linearly with the density ($E_0 \sim \rho$) and is proportional to $E_f A$ (where E_f is Young's modulus of the fiber material and $A \sim d^2$ is the area of the fiber cross-section) in the affine regime. In the non-affine regime $E_0 \sim E_f I \rho^q$, where q = 2 for the Voronoi structures[25,35] and q = 8 for 2D Mikado networks,[27,29,36] while I is the axial moment of inertia of the fiber cross-section ($I \sim d^4$). These scaling relations hold provided ρ is well above the transport percolation threshold for the respective stochastic geometry.

The degree of non-affinity is defined by a non-dimensional structural parameter, w, which combines the effect of ρ and d. In the Mikado case, $w = \log_{10}[(\rho L_0)^7 (d/4L_0)^2]$, while in the Voronoi case, $w = \log_{10}[\rho (d/4)^2]$. The non-affine to affine transition takes place in Mikado and Voronoi networks in the vicinity of $w_{NA-A} = 4.5$ and of $w_{NA-A} = -1.2$, respectively.[29,37] In this work we construct networks with a broad range of w values such to span the non-affine range and the non-affine to affine transition. We note that the majority of network materials, particularly the biological collagen-based networks, have parameters that place them in the non-affine category.

3. Results and discussion

3.1 Relaxation of networks with identical fibers

We consider first networks of fibers made from the same viscoelastic material, represented by a Maxwell model with relaxation time constant, τ_f. Stress relaxation following an imposed uniaxial strain of ε_0 = 3% is evaluated for Mikado and Voronoi networks with a broad range of w values in the non-affine and affine regimes. w is varied by changing ρ and d and we confirm that networks with different ρ and d, but with same w relax identically. Hence, the non-dimensional parameter w provides a sufficient representation of the structure in this problem and for this type of networks. Given the duality between linear elasticity and viscoelasticity, this is expected; note that w is also the unique parameter that controls the small strain stiffness, E_0, in networks of fibers made from the same material.

Fig. 2a shows stress relaxation curves for Mikado networks of w = 3.47 and 4.38, which correspond to the non-affine regime, $w < w_{NA-A}$, and w = 5.47 in the initial range of the affine regime. The time-dependent stress, $\sigma(t)$, is normalized by the stress at the onset of relaxation, σ_0. It is observed that relaxation is exponential at early times, regime in which networks with different w relax identically, but becomes slower at later times. To test whether the data conforms to a stretched exponential function (Kohlrausch relaxation) of the form

$$\sigma(t) = \sigma_0 \exp[-(t/\tau)^{\beta}], \quad (1)$$

we replot the curves in Fig. 2a as $y = \ln[-\ln(\sigma(t)/\sigma_0)]$ *vs.* $\ln t/\tau_f$, in Fig. 2b. If the stretched exponential is an adequate representation of the data, the plot must become linear, of slope equal to the stretch exponent, β, and intercept $\beta \ln \tau/\tau_f$.

Fig. 2b confirms the existence of two relaxation regimes: the first (regime I) is exponential (β = 1), while the second (regime II) is described by eqn (1), as also shown schematically in Fig. 2d. Mikado networks with different w lead to overlapping curves in regime I, that enter regime II at different transition times t_t marked by point O in Fig. 2d. For w in the affine regime, exponent β of regime II increases with w, as shown schematically in Fig. 2d, line OC. A similar behavior is observed for Voronoi networks, Fig. 2c.

For both Mikado and Voronoi cases, networks of increasing size were considered to check for size effects. With the models used to evaluate the data reported here being of edge size L (the total number of fibers in a typical Voronoi and Mikado network used is approximately 120 000 and 700, respectively), we considered models of size $2L$ and $4L$ and observed no difference in the relaxation curves, which indicates that the reported results are free of model size effects.

Similar phenomenology, including an initial exponential relaxation followed by slowing down of relaxation dynamics, is generally observed in glass forming systems in the vicinity of T_g;

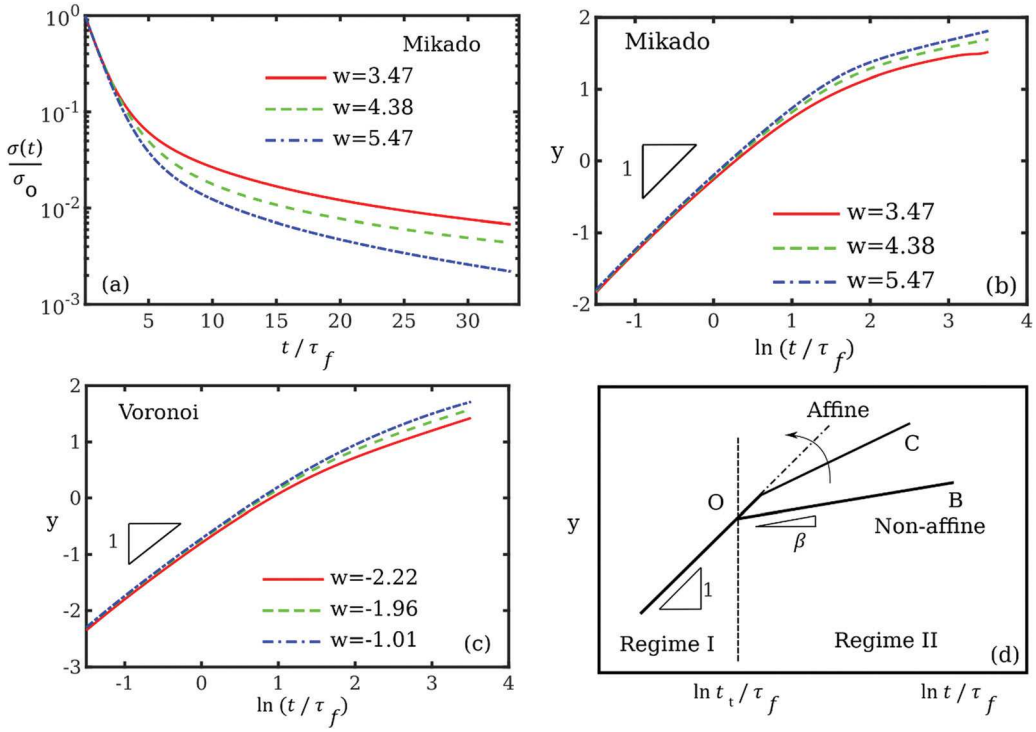

Fig. 2 (a) Semi-logarithmic representation of normalized stress *vs.* time relaxation curves for Mikado networks with w = 3.47, 4.38 and 5.47; (b) The data in (a) replotted as $y = \ln[-\ln(\sigma(t)/\sigma_0)]$ *vs.* $\ln t/\tau_f$; (c) similar data for Voronoi networks with $w = -2.22$, -1.96 and -1.01. Panel (d) shows a schematic of the curves in (b) and (c) emphasizing the two relaxation regimes and the associated parameters.

see reviews in ref. 38 and 39. The origin of the slowing down was debated in a large number of publications and was captured by models.[40] The control parameter in these cases is the temperature. For $T \gg T_g$, relaxation is exponential, while the stretched exponential function becomes dominant as T approaches T_g. The stretch exponent β was placed in relation to the fragility parameter, $m = \mathrm{d}\log\langle\tau\rangle/\mathrm{d}(T_g/T)$, which represents the departure of the temperature dependence of the mean relaxation time τ from the prediction of the Arrhenius function.[41] This establishes the common physical origin of the slowing down of relaxation and of fragility. The stretched exponent was also related to the dynamic free volume.[42] The non-equilibrium physics perspective on this phenomenon is based on the concept that spatial correlations of dynamics appear in disordered systems as they approach jammed states. Correlated local dynamics leads to slowing down of relaxation probed on scales larger than the correlation length, which itself increases in time.[39]

Similar phenomenology is observed here in an entirely athermal system and is introduced by the intrinsic structural heterogeneity of the network. This issue is discussed further in Section 3.2. The control parameter in this case is w, which represents the degree of heterogeneity. As opposed to thermal systems in the vicinity of the glass transition, here the heterogeneity is structural and does not evolve during relaxation.

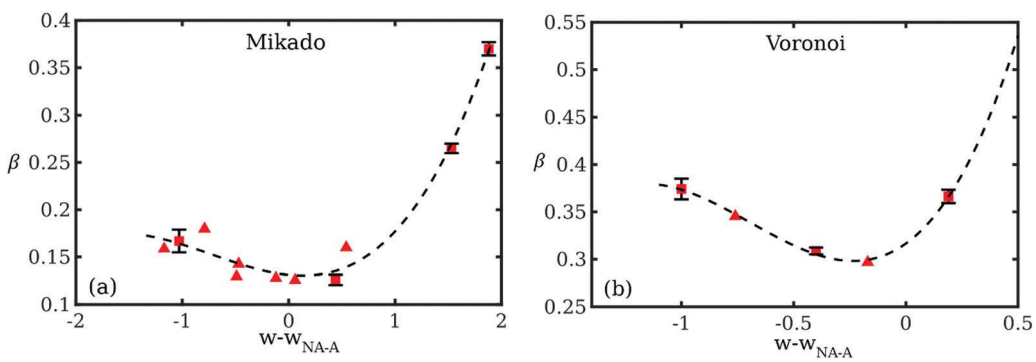

Fig. 3 (a) Variation of the stretch exponent with w for (a) Mikado and (b) Voronoi networks. Triangles represent single replica simulations. Squares indicate conditions for which 4 replicas (different realizations of the network) are considered and the bars represent standard error of β. The dashed lines represent fits with a polynomial of order 3 to the entire data set.

Fig. 3 shows the variation of the stretch exponent with w for Mikado (Fig. 3a) and Voronoi (Fig. 3b) networks. The triangles show all systems studied and the bars represent the standard error of a set of 4 replicas for each of the conditions indicated by square symbols. The data indicates well-defined minima at the transition between the non-affine and affine regimes, *i.e.* at $w = w_{NA-A}$. The smallest β is approximately 0.14 in the 2D Mikado case, and 0.3 in the 3D Voronoi case. β values for a large number of glass-forming polymers in the vicinity of glass transition are presented in.[41] β at T_g is generally larger than 0.5, but several systems exhibit low β, such as poly vinylchloride which has $\beta = 0.24$.

Lower values of β indicate that relaxation is more constrained by heterogeneity. The problem has two theoretical limits: in the limit of very small w, filaments have negligible bending stiffness. Since the bending mode is the softest, the axial mode is not engaged. This implies that interactions in the network are weak and hence fibers relax independently. In this limit, relaxation of the network should be identical to that of individual fibers, *i.e.* regime II in Fig. 2d is absent and $\beta = 1$ throughout the entire relaxation history. In the limit of large w, deformation is affine, which is equivalent to saying that the correlation length of the local relaxation modes diverges. The network is forced to relax as a homogeneous continuum. Hence, in this limit $\beta = 1$ and relaxation becomes exponential. This physical picture indicates that in the non-affine range, as w increases and the cooperativity of relaxation increases, β should decrease, while as the system moves into the affine regime, β should increase towards 1. This argument does not predict the value of w at which β reaches its minimum. The numerical study reported here indicates that, interestingly, the minimum β results at the transition between the non-affine and affine regimes, $w = w_{NA-A}$.

We turn now to the relaxation times, τ_I and τ_{II}, of regimes I and II, respectively. During regime I, $\sigma(t) = \sigma_0 \exp[-t/\tau_I]$, and τ_I is independent of w for both 2D and 3D networks. This is expected since the initial exponential regime corresponds to the independent relaxation of small networks subdomains. In the limit in which the size of these subdomains is equal to l_c, fibers relax independently and hence $\tau_I = \tau_f$. This limit is recovered in the present study for all Mikado networks considered. In the Voronoi case, τ_I is somewhat larger than τ_f ($\tau_I \approx 2\tau_f$), but it is independent of w, which supports the idea that regime I is not controlled by the network structure and parameters.

Fig. 4a shows the variation of the relaxation time constant in regime II, τ_{II}, with w, for all Mikado and Voronoi networks considered in Fig. 3. τ_{II} is normalized by τ_I and the horizontal axis represents $w - w_{NA-A}$. Just like β, τ_{II} has a minimum at $w = w_{NA-A}$. Fig. 4b shows the transition time between regimes I and II, t_t, function of $w - w_{NA-A}$. The transition time is normalized by τ_I of the respective network. The transition time increases for w in the non-affine regime, while in the affine regime it remains approximately constant. At $w = w_{NA-A}$, $t_t \approx 3\tau_I$ in the Voronoi case and $t_t \approx 4\tau_I$ in the Mikado case.

3.2 Network-scale dynamics

In order to understand the mechanism of relaxation, it is useful to observe the local relaxation dynamics. To this end, we work with Mikado networks (such to facilitate visualization) and compute the velocity of each crosslink throughout the relaxation history. The domain is divided in square patches of size $4l_c$ and the crosslink velocities are averaged over each patch. Fig. 5 shows the resulting velocity field for a non-affine network with $w = 3.47$ at time $t/t_t = 8.3$, *i.e.* into regime II. This network is loaded in tension to $\varepsilon_0 = 3\%$ in the horizontal direction, after which the vertical boundaries of the model are held fixed, while the upper and lower boundaries are kept traction free. The field shown in Fig. 5 is normalized by the mean $\bar{v}$ of the distribution of velocity magnitudes $v = |\mathbf{v}|$.

Fig. 5 shows a complex relaxation pattern which demonstrates that the structure is strongly mechanically heterogeneous. Based on field v we compute the symmetric component of the velocity gradient tensor $\nabla\mathbf{v}$, *i.e.* $\dot{\varepsilon} = (\nabla\mathbf{v} + \nabla\mathbf{v}^T)/2$, and further compute the hydrostatic and deviatoric components of $\dot{\varepsilon}$. The hydrostatic component is $\dot{\varepsilon}_h\mathbf{I}$, where

$$\dot{\varepsilon}_h = (\dot{\varepsilon}_{11} + \dot{\varepsilon}_{22})/2 = ((\nabla\mathbf{v})_{11} + (\nabla\mathbf{v})_{22})/2 \quad (2)$$

The deviatoric component, $\dot{\varepsilon} - \dot{\varepsilon}_h\mathbf{I}$, has two eigenvalues of equal magnitude and opposite sign. We take the positive

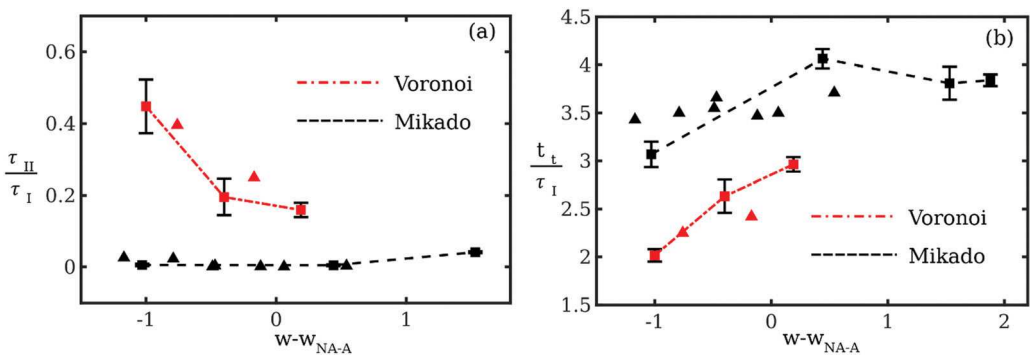

Fig. 4 (a) Variation of the relaxation time constant in regime II, τ_{II}, with w for all Mikado and Voronoi networks considered in Fig. 3. (b) Transition time between regimes I and II, t_t, function of $w - w_{NA-A}$. Triangles represent single replica simulations. Squares indicate conditions for which 4 replicas (different realizations of the network) are considered and the bars represent standard error. The lines connect the square symbols.

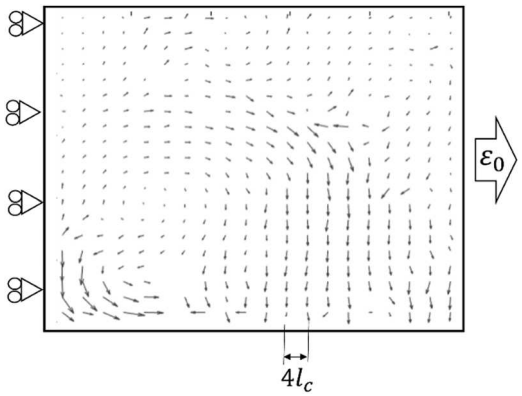

Fig. 5 Velocity field for a non-affine network with $w = 3.47$ at time $t/t_t = 8.3$. The velocities are coarse grained on the scale of square sub-domains of size $4l_c$.

eigenvalue which, in terms of components of ∇v is given by

$$\dot{\varepsilon}_s = \frac{1}{2}\sqrt{\left((\nabla \mathbf{v})_{11} - (\nabla \mathbf{v})_{22}\right)^2 + \left((\nabla \mathbf{v})_{12} + (\nabla \mathbf{v})_{21}\right)^2} \qquad (3)$$

to be representative for the shear strain rate of the relaxation field. Further, we evaluate the spin, which is the only nonzero component of the anti-symmetric part of the velocity gradient, $S = ((\nabla v)_{12} - (\nabla v)_{21})/2$.

We use the scalar quantities $\dot{\varepsilon}_h$, $\dot{\varepsilon}_s$ and S to characterize the rates of volumetric and shear relaxation strains and the angular velocity of the relaxation field, respectively. Let $\bar{\dot{\varepsilon}}_h$, $\bar{\dot{\varepsilon}}_s$ and $\bar{S}$ represent the averages of the respective fields over the entire problem domain, and $\sigma_{\dot{\varepsilon}h}$, $\sigma_{\dot{\varepsilon}s}$ and σ_S be the corresponding standard deviations. The coefficients of variation of these fields are computed as $CV_{\dot{\varepsilon}_h} = \sigma_{\dot{\varepsilon}_s}/\bar{\dot{\varepsilon}}_h$, $CV_{D_s} = \sigma_{\dot{\varepsilon}_s}/\bar{\dot{\varepsilon}}_h$ and $CV_S = \sigma_S/\bar{S}$.

Fig. 6a show the variation of the means of the three scalar measures during the relaxation of the network whose velocity field is shown in Fig. 5 ($w = 3.47$); $\bar{\dot{\varepsilon}}_h$, $\bar{\dot{\varepsilon}}_s$ and $\bar{S}$ are rendered non-dimensional by normalization with $\bar{v}/l_c$. We observe that, while all three fields $\dot{\varepsilon}_h$, $\dot{\varepsilon}_s$ and S are non-zero, relaxation is controlled by the shear mode, as $\bar{\dot{\varepsilon}}_s$ is one order of magnitude larger than the dilatational and spin components, $\bar{\dot{\varepsilon}}_h$ and $\bar{S}$, at all times. This observation is not unexpected since the shear mode is softer than the dilatational mode. We observe that the contribution of the spin is similar to that of the dilatational mode. Further, we observe (not shown in Fig. 6a) that the time variation of $\bar{\dot{\varepsilon}}_s$ is similar to that of the stress shown in Fig. 2b, *i.e.* it exhibits a stretched exponential time dependence at times larger than t_t. Based on these observations, we use further the shear component to characterize the relaxation.

The coefficient of variation of the shear rate, $CV_{\dot{\varepsilon}_s}$, provides a measure of the magnitude of dynamic heterogeneity during relaxation. Fig. 6b shows the time and w dependence of $CV_{\dot{\varepsilon}_s}$. Each curve represents $CV_{\dot{\varepsilon}_s}(w)$ computed at a given time, t/τ_f. The main observation is that all curves have a maximum at $w = w_{NA-A} = 4.5$. This demonstrates that dynamic heterogeneity reaches a maximum at the non-affine to affine transition, and provides a physical justification for the presence of a minimum in the stretch exponent β at $w = w_{NA-A}$, Fig. 3. Comparing the three curves indicates the evolution of the shear rate field heterogeneity during relaxation. We observe that for $t > t_t$, the fluctuation magnitude, as measured by $CV_{\dot{\varepsilon}_s}$, does not vary in time. This depicts a physical picture quite different from that of thermal glass formers close to T_g. The heterogeneity of the relaxation field emerges from the structural heterogeneity of the network, which does not change in time. Since parameter w represents the degree of structural disorder, it also controls the magnitude of dynamic heterogeneity, much like the temperature is the control parameter in thermal systems.

It is interesting to put this result in relation with polymeric glass formers with network structure. Relaxation in these systems is controlled by the dynamic heterogeneity which becomes more pronounced close to the glass transition. In general terms, relaxation is thought to be controlled by packing. However, the structure of the network is expected to play a role. One may modify w of these networks by increasing the stiffness of the polymer backbone (equivalent to increasing d in athermal networks). Considering that such networks belong to the non-affine range, the present results indicate that increasing the chain stiffness should lead to the decrease of the stretch exponent, β. Based on the results in,[41] decreasing β should be associated with an increase of fragility, which implies a shift of the temperature dependence of relaxation (and viscosity) from

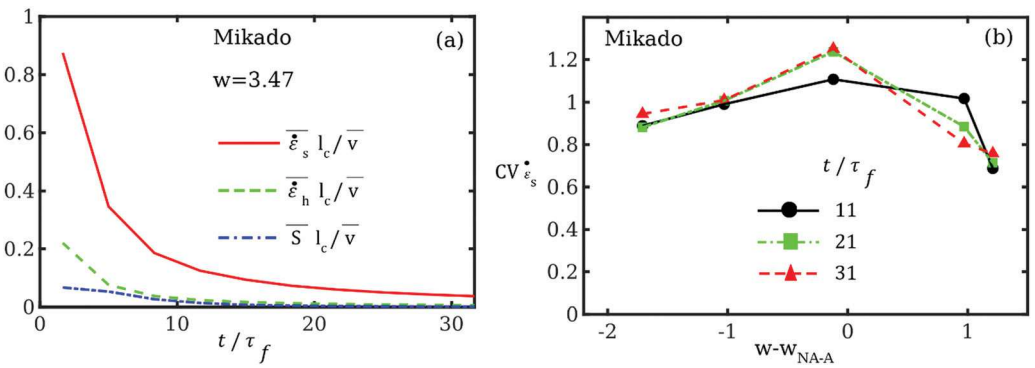

Fig. 6 (a) Variation of $\bar{\dot{\varepsilon}}_h$, $\bar{\dot{\varepsilon}}_s$ and $\bar{S}$ during the relaxation of the network whose velocity field is shown in Fig. 5 ($w = 3.47$). (b) Time and w dependence of $CV_{\dot{\varepsilon}_s}$.

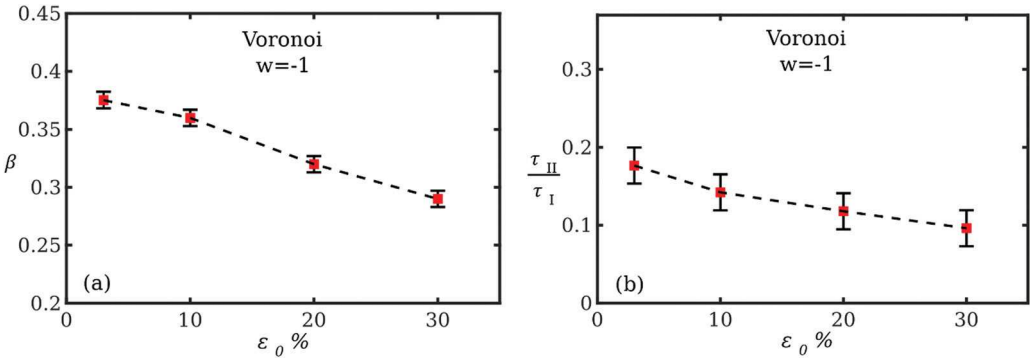

Fig. 7 Variation of the (a) stretch exponent and (b) relaxation time constant, τ_{II}, with the pre-strain, ε_0, for a 3D Voronoi network with $w = -1$. The bars represent standard error for 4 replicas of the respective networks. τ_{II} is normalized by the relaxation time of regime I, τ_I.

Arrhenius to Vogel–Fulcher–Tammann-type. Such dependence of fragility on the chain stiffness was observed recently in a vitrimer system,[43] which provides support of the conjecture introduced here that both the dynamic heterogeneity (as in monatomic glasses) and the structural heterogeneity (as in athermal networks) control relaxation in network-like, thermal polymeric glass formers.

3.3 Effect of pre-strain

Networks are usually subjected to large strains. Since their elasticity is non-linear, their viscoelasticity is also expected to be non-linear. In both cases, non-linearity is of geometric type and emerges from the structural re-organization of the network under large strains. For example, ref. 13 and 44 report that in collagen networks the time-dependent modulus $E(t)/E(0)$ is independent of the initial strain at relatively small strain levels, but the relaxation time constants decrease (relaxation becomes faster) with increasing ε_0.

To test the effect of large strains on relaxation we consider a Voronoi network with $w = -1$ and vary the pre-strain parameter ε_0 from 3% to 30%. The two relaxation regimes reported in Fig. 2 are observed for all values of ε_0 considered, with the stress being described by exponential and stretched exponential functions in regimes I and II, respectively. The stretch exponent becomes a weakly decreasing function of ε_0, as shown in Fig. 7a. The relaxation time constant of regime II also decreases with ε_0, as shown in Fig. 7b, and in agreement with experimental observations in collagen networks.

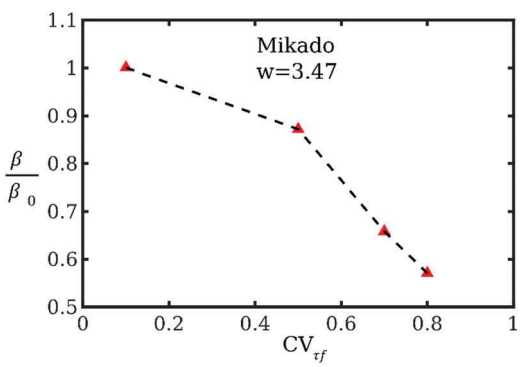

Fig. 8 Variation of the stretch exponent with the coefficient of variation of the distribution of fiber relaxation times, CV_{τ_f}. The stretch exponent of composite networks is normalized by that of networks in which all fibers have the same relaxation time constant (denoted here by β_0), equal to the mean of the distribution of fiber relaxation time constants in the composite network case, $\bar{\tau}_f$.

3.4 Relaxation of networks with non-identical fibers

Many network materials are composite, in the sense that material properties of fibers vary from fiber to fiber. Such variability adds to the intrinsic structural stochasticity of the network, increasing the degree of heterogeneity. Therefore, it becomes of interest to determine to what extent the results presented in the preceding sections apply to composite networks.

To this end, we consider Mikado networks of $w = 3.47$ in which all fibers have the same Young's modulus, E_f, but the relaxation time constant, τ_f, is selected from a Gamma distribution, $p(\tau_f)$. The mean of the distribution, $\bar{\tau}_f$, is kept fixed and equal to the value considered above for the analysis of networks composed from fibers with identical material properties. The coefficient of variation of the distribution, CV_{τ_f}, is kept as parameter and varied in the interval [0, 0.8].

A similar analysis pertaining to elastic networks was reported in,[45] where the fiber material was linear elastic and fiber Young's modulus was selected from a distribution. The mean of the distribution was kept constant and the variance was increased such to evaluate the effect of increasing heterogeneity on network modulus. It was concluded that the overall network stiffness decreases with increasing variance, a result which also applies to the elasticity of continuum composites.[46]

We observe that relaxation preserves the two regimes shown in Fig. 2, with the first regime being exponential and the second being described by a stretched exponential with exponent β. Fig. 8 shows the variation of β with the magnitude of the pre-strain, ε_0; β is normalized by the stretch exponent β_0 of the same network in which all fibers have the same relaxation time constant, equal to $\bar{\tau}_f$. The stretch exponent decreases with increasing the variability of the relaxation time of individual fibers. This is expected, since increasing CV_{τ_f} leads to increased structural heterogeneity. The result underlines, once again, the

causal relationship between the stretched exponential and the structural heterogeneity of the network.

4. Conclusions

In this work we study the component of the relaxation behavior of network materials associated with the viscoelasticity of the fiber material. We focus on athermal 2D and 3D stochastic networks and observe that relaxation has two regimes, of which the first is exponential, while the second is of Kohlrausch type. The relationship between the stretch exponent and the structural parameter w, which defines the degree of non-affinity of the network, is established. It is seen that relaxation is slowest (smallest stretch exponent) for networks at the transition between the affine and non-affine regimes. The physical origin of the slowdown is related to the structural heterogeneity of the network. In composite networks in which the relaxation time of individual fibers is different from fiber to fiber, relaxation slows down further due to the enhanced structural heterogeneity. We discuss that these findings are similar to observations made in glass forming systems. However, while the dynamic heterogeneity in such systems evolves during relaxation, the heterogeneity in networks is structural and is not evolving in time. The control parameter of the relaxation process, which in thermal system is the temperature, is identified in athermal networks to be the non-dimensional structural parameter w.

Conflicts of interest

The authors have no competing interests to declare.

Acknowledgements

This work was supported by the National Science Foundation through grants CMMI-2007909 and CMMI-2022489.

References

1 B. Babaei, S. D. Abramowitch, E. L. Elson, S. Thomopoulos and G. M. Genin, *J. R. Soc., Interface*, 2015, **12**, 20150707.
2 P. de Buhan, X. Chateau and L. Dormieux, *European Journal of Mechanics - A/Solids*, 1998, **17**, 909–921.
3 V. C. Mow, S. C. Kuei, W. M. Lai and C. G. Armstrong, *J. Biomech. Eng.*, 1980, **102**, 73–84.
4 K. L. Ngai, S. Capaccioli and D. J. Plazek, in *The Science and Technology of Rubber*, ed. B. Erman, J. E. Mark and C. M. Roland, Academic Press Elsevier Science & Technology, Waltham, MA, USA, 4th edn, 2013, pp. 193–284.
5 L. G. Baxandall, *Macromolecules*, 1989, **22**, 1982–1988.
6 O. Lieleg, M. M. A. E. Claessens, Y. Luan and A. R. Bausch, *Phys. Rev. Lett.*, 2008, **101**, 108101.
7 R. A. Pethrick, *Polym. Int.*, 2004, **53**, 1394–1395.
8 G. J. Tortora and B. Derrickson, *Principles of anatomy & physiology*, Wiley, Danvers, MA, 2014.
9 M. A. Biot, *J. Appl. Phys.*, 1941, **12**, 155–164.
10 Y. Hu and Z. Suo, *Acta Mech. Solida Sin.*, 2012, **25**, 441–458.
11 N. Zolfaghari, M. Moghimi Zand and M. R. K. Mofrad, *Soft Mater.*, 2020, **18**, 373–385.
12 R. Y. Dhume and V. H. Barocas, *Acta Biomater.*, 2019, **87**, 245–255.
13 B. Xu, H. Li and Y. Zhang, *J. Biomech. Eng.*, 2013, **135**, 054501.
14 K. M. Pryse, A. Nekouzadeh, G. M. Genin, E. L. Elson and G. I. Zahalak, *Ann. Biomed. Eng.*, 2003, **31**, 1287–1296.
15 B. Babaei, A. Davarian, K. M. Pryse, E. L. Elson and G. M. Genin, *J. Mech. Behav. Biomed. Mater.*, 2016, **55**, 32–41.
16 K. Komatsu, *J. Dent. Biomech.*, 2010, **1**, 1–18.
17 J. E. Wagenseil, T. Wakatsuki, R. J. Okamoto, G. I. Zahalak and E. L. Elson, *J. Biomech. Eng.*, 2003, **125**, 719–725.
18 C. Y. Hui and V. Muralidharan, *J. Chem. Phys.*, 2005, **123**, 154905.
19 W. C. Lin, K. R. Shull, C. Y. Hui and Y. Y. Lin, *J. Chem. Phys.*, 2007, **127**, 094906.
20 M. Galli, K. S. C. Comley, T. A. V. Shean and M. L. Oyen, *J. Mater. Res.*, 2009, **24**, 973–979.
21 Y. Hu, X. Zhao, J. J. Vlassak and Z. Suo, *Appl. Phys. Lett.*, 2010, **96**, 121904.
22 R. Jubera, A. Ridruejo, C. González and J. Llorca, *Mech. Mater.*, 2014, **74**, 14–25.
23 R. R. Duling, R. B. Dupaix, N. Katsube and J. Lannutti, *J. Biomech. Eng.*, 2008, **130**, 011006.
24 C. P. Broedersz, M. Sheinman and F. C. MacKintosh, *Phys. Rev. Lett.*, 2012, **108**, 078102.
25 M. R. Islam and R. C. Picu, *J. Appl. Mech.*, 2018, **85**, 081011.
26 R. C. Picu, S. Deogekar and M. R. Islam, *J. Biomech. Eng.*, 2018, **140**, 021002.
27 D. A. Head, A. J. Levine and F. C. MacKintosh, *Phys. Rev. E: Stat., Nonlinear, Soft Matter Phys.*, 2003, **68**, 061907.
28 C. Heussinger and E. Frey, *Phys. Rev. E: Stat., Nonlinear, Soft Matter Phys.*, 2007, **75**, 011917.
29 A. S. Shahsavari and R. C. Picu, *Int. J. Solids Struct.*, 2013, **50**, 3332–3338.
30 O. Kallmes and H. Corte, *Tappi J.*, 1960, **43**, 737–752.
31 S. Deogekar, Z. Yan and R. C. Picu, *J. Appl. Mech.*, 2019, **86**, 081010.
32 S. Deogekar, M. R. Islam and R. C. Picu, *Int. J. Solids Struct.*, 2019, **168**, 194–202.
33 R. C. Picu, *Soft Matter*, 2011, **7**, 6768–6785.
34 C. P. Broedersz and F. C. Mackintosh, *Rev. Mod. Phys.*, 2014, **86**, 995–1036.
35 L. Gibson and M. F. Ashby, *Cellular solids: structure and properties*, Cambridge Univ. Press, Cambridge, 1988.
36 S. Deogekar and R. C. Picu, *Phys. Rev. E*, 2017, **95**, 10–20.
37 S. Deogekar and R. C. Picu, *J. Mech. Phys. Solids*, 2018, **116**, 1–16.
38 A. K. Rajagopal, K. L. Ngai and S. Teitler, *J. Non-Cryst. Solids*, 1991, **131–133**, 282–288.
39 D. Chandler and J. P. Garrahan, *Annu. Rev. Phys. Chem.*, 2010, **61**, 191–217.
40 L. M. C. Janssen, *Front. Phys.*, 2018, **6**, 97.

41 R. Böhmer, K. L. Ngai, C. A. Angell and D. J. Plazek, *J. Chem. Phys.*, 1993, **99**, 4201–4209.
42 V. P. Privalko, *J. Non-Cryst. Solids*, 1999, **255**, 259–263.
43 R. G. Ricarte and S. Shanbhag, *Macromolecules*, 2021, **54**, 3304–3320.
44 S. Nam, K. H. Hu, M. J. Butte and O. Chaudhuri, *Proc. Natl. Acad. Sci. U. S. A.*, 2016, **113**, 5492–5497.
45 E. Ban, V. H. Barocas, M. S. Shephard and R. C. Picu, *J. Mech. Phys. Solids*, 2016, **87**, 38–50.
46 E. Ban, *Mech. Mater.*, 2019, **129**, 139–147.

